Time Dependent Dirac Equation FEM Solutions for Relativistic Quantum Mechanics

A. J. Kalinowski*[1]
[1]Consultant
*Corresponding author: East Lyme CT 06333, kalinoaj@aol.com

Abstract: COMSOL is used for obtaining the quantum mechanics wave function $\{\Psi_m(x,y,z,t)\}$ as a solution to the *time dependent* Dirac equation. The probability determination of a particle being at a spatial point can be treated by a) the "matrix mechanics formulation" or b) the "wave function formulation". The latter approach is used herein, because it involves solving field partial differential equations, thus is directly adaptable to COMSOL.

Keywords: Quantum Mechanics, Time Dependent Dirac Equation, Wave Propagation.

1. Introduction

The purpose of this paper is to illustrate the use of COMSOL for obtaining the quantum mechanics wave function $\Psi_m(x,y,z,t)$ (representing *matter waves*) as a solution to the *time dependent* Dirac equation. Quantum mechanics solutions for the probability of a particle being at a particular point in space are usually treated through: a) the "matrix mechanics formulation" originated by Werner Heisenberg or b) the "wave function formulation" originated by Erwin Schrödinger. The latter approach is the one used herein, mainly because it involves solving field partial differential equations, and therefore is directly adaptable to COMSOL.

The Dirac equation is employed in particle physics and historically provided the first combined application of quantum mechanics and relativity theory by introducing a four component wave function $\{\Psi_m\}$, m=1,2,3,4 (e.g. in contrast to the one component Schrödinger wave function Ψ or Klein-Gordon wave function Ψ). Historically, $\{\Psi_m\}$ described the behavior of fermion type particles (e.g., electrons) and further predicted the existence of antiparticles (e.g., positrons) even before they were observed experimentally. Use of COMSOL MULTIPHYSICS®: the Coefficient-Form PDE "*time dependent*" study is employed. When the wave vector **k** lies in the xy plane, the four component $\{\Psi_m\}$ simplifies into two components for m=1&4. COMSOL is then used for obtaining the transient 2-D $\{\Psi_1(x,y,t),\Psi_4(x,y,t)\}$ wave propagation evolution as a solution to exp(-iωt) upfield boundary driven models at frequency ω. There is one example in the COMSOL archives for solving the *time independent* Quantum Mechanics Dirac wave function [2]; however, the problems addressed here are the first COMSOL application towards solving the *time dependent* Dirac equation. Three validation examples (using comparisons to exact transient solutions when available or to steady state limit solutions as second choice alternative) are presented, followed by more complex examples without an available exact solution for comparison.

2. Governing Equations

Governing equations for the behavior of a free fermion particle, of mass *m,* are represented by the *time dependent* quantum mechanics Dirac equations (with wave function $\{\Psi_m(x,y,z,t)\}$ as the dependent variable) and are given by [1]:

$$\begin{aligned}
&\frac{1}{c}\frac{\partial\Psi_1}{\partial t}+\frac{\partial\Psi_4}{\partial x}-i\frac{\partial\Psi_4}{\partial y}+\frac{\partial\Psi_3}{\partial z}+iM\Psi_1=0\\
&\frac{1}{c}\frac{\partial\Psi_2}{\partial t}+\frac{\partial\Psi_3}{\partial x}+i\frac{\partial\Psi_3}{\partial y}-\frac{\partial\Psi_4}{\partial z}+iM\Psi_2=0\\
&\frac{1}{c}\frac{\partial\Psi_3}{\partial t}+\frac{\partial\Psi_2}{\partial x}-i\frac{\partial\Psi_2}{\partial y}+\frac{\partial\Psi_1}{\partial z}-iM\Psi_3=0\\
&\frac{1}{c}\frac{\partial\Psi_4}{\partial t}+\frac{\partial\Psi_1}{\partial x}+i\frac{\partial\Psi_1}{\partial y}-\frac{\partial\Psi_2}{\partial z}-iM\Psi_4=0
\end{aligned} \qquad (1)$$

with $M=mc/\hbar$, c= speed of light, $\hbar = h/(2\pi)$, (where *h* is Planck's constant), and $i=\sqrt{(-1)}$.

2.1 Transient *time dependent* form

A 2-D form of governing Eqs.(1) are solved in *time dependent* problems using the COMSOL MULTIPHYSICS® Coefficient-Form PDE "T*ime dependent*" studies option. Two dimensional solutions are sought where the wave function depends on spatial coordinates x,y. Therefore gradients in the z direction drop out and the $\{\Psi_1(x,y,t),\Psi_4(x,y,t)\}$ components are solved with

just the 1st and 4th coupled equations of Eqs.(1):

$$\frac{1}{c}\frac{\partial \Psi_1}{\partial t}+\frac{\partial \Psi_4}{\partial x}-i\frac{\partial \Psi_4}{\partial y}+iM\Psi_1=0 \qquad (2a)$$

$$\frac{1}{c}\frac{\partial \Psi_4}{\partial t}+\frac{\partial \Psi_1}{\partial x}+i\frac{\partial \Psi_1}{\partial y}-iM\Psi_4=0 \qquad (2b)$$

In [2], the *coupled time independent* form these equations were solved as two simultaneous pde's for Ψ_1&Ψ_4 . A different uncoupled approach is used herein, where after differentiating Eq.(2b) with $\partial(\ )/\partial x$ & $\partial(\ )/\partial y$ (while introducing scaled time and spatial *primed* independent variables x′,y′,t′); the Ψ_4 terms are eliminated using Eq.(2a), resulting in the Eq.(3) pde for Ψ_1 alone (we omit primes on dependent variables Ψ_1, Ψ_4, ρ_d hereon) :

$$\frac{\partial^2 \Psi_1}{\partial t'^2}-c'^2\left(\frac{\partial^2 \Psi_1}{\partial x'^2}+\frac{\partial^2 \Psi_1}{\partial y'^2}\right)+(c'M')^2\Psi_1=0 \qquad (3)$$

$$\text{where} \quad t=t'\mathbf{T} \ , x=x'\mathbf{L}, \ y=y'\mathbf{L} \qquad (3a)$$

$$\text{and} \quad c'\equiv c\mathbf{T}/\mathbf{L} \quad M'\equiv M\mathbf{L} \quad c'M'=cM\mathbf{T} \qquad (3b)$$

In passing, it is noted that Eq.(3) is the same as the relativistic 2-D "Klein-Gordon equation" [1].

After solving Eq.(3) for Ψ_1 (and its spatial derivatives), at an arbitrary point {x′=X′,y′=Y′}, primed Eq.(2b) is used to post process Ψ_4 . It can be obtained from the first order in time differential equation:

$$\frac{d\Psi_4}{dt'}-\gamma'\Psi_4=g(X',Y',t'); \quad \gamma'=ic'M' \qquad (4)$$

$$g(X',Y',t')=-c'\left(i\frac{\partial \Psi_1(X',Y',t')}{\partial y'}+\frac{\partial \Psi_1(X',Y',t')}{\partial x'}\right)$$

Equation (4) is solved with Laplace transforms resulting in Eq.(5) (with Ψ_4(X′,Y′,+0)=0 downfield):

$$\Psi_4(X',Y',t')=e^{+\gamma' t'}\left(\Psi_4(X',Y',+0)+\int_0^{t'} g(X',Y',\tau')e^{-\gamma'\tau}d\tau'\right) \qquad (5)$$

2.2 Steady State *time independent* form

Substitute Steady State (S.S.) Eqs.(6) into

$$\Psi_1(x',y',t')=\psi_1(x',y')e^{-i\omega' t'} \qquad (6)$$
$$\Psi_4(x',y',t')=\psi_4(x',y')e^{-i\omega' t'}$$

Eq.(3), and Eq.(2b), to obtain the Helmholtz like

$$\left(\frac{\partial^2 \psi_1}{\partial x'^2}+\frac{\partial^2 \psi_1}{\partial y'^2}\right)+\left(\left(\frac{\omega'}{c'}\right)^2-M'^2\right)\psi_1=0 \qquad (7)$$

pde Eq.(7) for solving ψ_1(x′,y′) .

Employing the steady state version of Eq.(2b) at arbitrary point x′=X′, y′=Y′, the following algebraic Eq.(8) is used for post processing ψ_4 :

$$\psi_4(X',Y')=\left(\frac{\partial \psi_1(X',Y')}{\partial y'}-i\frac{\partial \psi_1(X',Y')}{\partial x'}\right)/\left(M'+\frac{\omega'}{c'}\right) \qquad (8)$$

(use stored $\partial\psi_1/\partial$x′, $\partial\psi_1/\partial$y′ from Eq.(7) FEM sol.) .

2.3 Selection of drive frequency ω and scaling parameters T,L

Frequency selection: De Broglie's photon-to-particle extension of Planck's relation between particle energy E_p and angular frequency ω (i.e. $E_p=\hbar\omega$), along with the *relativistic* relation between E_p and velocity [1], $E_p=mc^2/\sqrt{(1-\beta^2)}$, gives:

$$\omega=\frac{E_p}{\hbar}=cM/\sqrt{1-\beta^2} \ ; \qquad \beta=v_p/c \qquad (9)$$

for selecting the particle frequency in terms of the particle velocity v_p via the speed parameter β.

Scaling Parameters Selection: The scale of the solution domain is such that the numerical size of both time and space variables are extremely small in say standard CGS units. FEM models were solved directly in CGS units in [2] and [4]. However during the post processing plots phase, time and length scales were normalized by the time period $T_p=2\pi/\omega$ and spatial wave length $\lambda_p=2\pi/k$ (k is wave number) respectively of the dominant propagating wave in the problem. Equations (3-8) in the scaled prime variables are valid for *any* unit consistent values of (**T**,**L**), however a convenient choice is to use the time period T_p and wave length λ_p of a propagating Dirac Equation plane wave. The magnitude of all of the *primed variables* in the FEM models (both in model building, solving, and post processing) are then nice size numbers.

The S.S. exact solution to *unscaled* Eqs.(2), for a plane wave (inclined θ_{inc} to the x axis, of frequency ω, and traveling in unit vector direction **n,** with position vector **r**=x**i**+y**j**), is given by [1]):

$$\begin{Bmatrix}\psi_1\\ \psi_4\end{Bmatrix}=A\left\{\frac{1}{\frac{exp[i\theta_{inc}]}{R}}\right\}exp[ik\hat{\rho}] \quad ;\hat{\rho}=\vec{n}\cdot\vec{r} \qquad (10)$$

$$k=\sqrt{(\omega/c)^2-M^2}; \ R=\frac{k}{(\omega/c)-M} \qquad (11)$$

where A is an arbitrary constant.

As an example, for a plane wave traveling in the +x direction, set **n**= x**i,** θ_{inc}=0, thus $\rho\hat{}$=x; whereas

for a wave in the -x dir., set **n= -xi,** $\theta_{inc}=\pi$, thus $\rho\hat{}=-x$.

Therefore after selecting Eq.(9) driver frequency ω, the following scale values for $\mathbf{T},\mathbf{L}$ are defined:

$$\mathbf{T}=2\pi/\omega \quad \mathbf{L}=2\pi/k=2\pi/\sqrt{(\omega/c)^2-M^2} \qquad (12a)$$

and primed ω',k' are: $\omega'=\omega\mathbf{T} \quad k'=k\mathbf{L}$ (12b)

3. Method

The Dirac equation problems are solved in the time domain by driving an upfield face of a model (that is initially at a zero wave function state) with exp(-i$\omega' t'$) harmonic loadings, and then track the ensuing waves that propagate towards the downfield end of the model.

3.1 FEM Boundary Conditions

FEM Wave Generation Driven Surface: transient solutions are generated by driving the upfield surfaces with time harmonic loadings of the form

$$\Psi_1(x'_s,y'_s,t')=\psi_1(x'_s,y'_s)f(t')e^{-i\omega' t'} \qquad (13)$$

where $f(t')$ is a gradual time increasing multiplier on the harmonic driver and $\psi_1(x'_s,y'_s)$ is the wave function distribution (typically set = 1.0) at surface points $\{x'_s,y'_s\}$. This gradual increase is to help minimize any suddenly applied loading effects. Specifically, the $f(t')$ time portion is given by:

$$f(t')=U_2(t')[U_3(t')+U_4(t')\exp(\alpha'(t'-t'_c))] \qquad (14)$$
$$U_3(t')=0 \;\; t'<t'_c \;;\; =1/2 \;\; t'=t'_c \;;\; =1 \;\; t'>t'_c$$
$$U_4(t')=1 \;\; t'<t'_c \;;\; =1/2 \;\; t'=t'_c \;;\; =0 \;\; t'>t'_c$$
$$U_2(t')=0 \;\; t'<0 \;\; ;=2\frac{t'^2}{t'^2_w}[\frac{3}{2}-\frac{t'}{t'_w}] \;\; 0\le t'\le t'_w \;;$$
$$=1 \;\; t'>t'_w$$

with, for example, shaping parameters of :

$$\alpha'=-\ln(\varepsilon_0)/t'_c \;;\; t'_c=N_c \;; \qquad (15)$$
$$N_c=2 \;;\; \varepsilon_0=.05 \;;\; t'_w=0.1$$

First $f(t')$ exponentially increases from ε_0 to 1.0 over N_c time cycles (the [ ] bracket term in first of Eqs.(14)). Then using transition term $U_2(t')$, the starting value, $f(0)=\varepsilon_0$, is made zero by blending $f(0)=0$ into $f(t'_w)$ with a cubic "s-shaped" curve ending at $t'=t'_w$. The shape of the input driver, using the parameters given in Eq.(15), is shown in Fig.(1a). These are the same parameters used in the Schrödinger equation time dependent solutions [4], that led to a smooth buildup of the surface driver. In Fig.(1b), the FFT of the real part of the Ψ_1 driver shows that the dominant primed frequency is at $f'=1.0$.

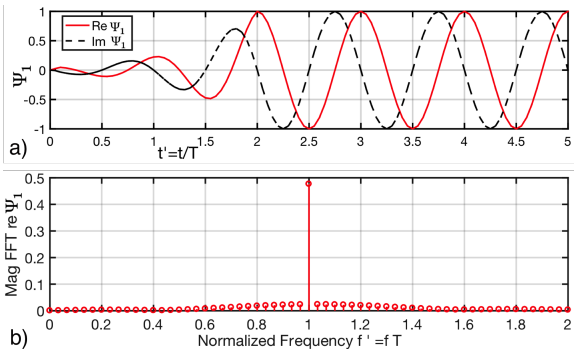

Figure 1. FEM Wave Generation Driver

FEM Model Termination Surfaces:

(i) absorbing B.C. : transient solutions are often terminated with some kind of wave absorbing boundary condition such as a plane wave absorber like:

$$\vec{n}\cdot\vec{\nabla}(\Psi_1(x',y',t'))=ik'\Psi_1(x',y',t') \qquad (16)$$

where the unit vector **n** is normal to the absorbing surface and k' is the wave number of the wave to be absorbed. However an advantage of the transient solution approach is that unlike the time independent steady state solutions, the transient solutions can be terminated at a time even before the propagating wave hits the downfield boundary. Equation(16) can be enforced in COMSOL with the *Elemental Constraint Method* Option, using the *Flux/Source Boundary Condition* with the source term g turned off.

(ii) soft B.C. : $\Psi_1(x'_s,y'_s,t')=0$, at surface points $\{x'_s,y'_s\}$

(iii) hard B.C. : normal grad. $\mathbf{n}\cdot\nabla\Psi_1(x'_s,y'_s,t')=0$, at surface points $\{x'_s,y'_s\}$, where **n** is a unit normal vector to the hard surface. This constraint can be enforced in COMSOL with the *Elemental Constraint Method* Option, using the *Flux/Source Boundary Condition* with both the source term g and flux term q turned off.

3.2 FEM Initial Conditions

The FEM model is started from rest throughout the entire spatial domain $\mathcal{D}$, therefore:

$$\Psi_1(x',y',0)=0 \;;\; \frac{\partial\Psi_1(x',y',0)}{\partial t'}=0 \;\; all\; x',y' \text{ in } \mathcal{D} \qquad (17)$$

It is noted that because of the manner Eq.(13) is constructed, evaluating it at $t'=0$ is consistent with Eqs.(17) for both $\Psi_1(x'_s,y'_s,0)$ and $\partial\Psi_1(x'_s,y'_s,0)/\partial t'$.

3.3 Probability Computation

The wave function $\{\Psi_1(x',y',t'),\Psi_4(x',y',t')\}$ can be used to compute the probability $P_{\Delta A}$ of a particle being in a finite area zone, $\Delta A'$, of space for 2-D models. Firstly, the probability density $\rho_d(x',y',t')$ is defined as the probability per unit area of the particle being at a particular spatial point $\{x',y'\}$, and is given [1] by Eq.(18):

$$\rho_d(x',y',t') = |\Psi_1|^2 + |\Psi_4|^2 \qquad (18)$$

$$P_{\Delta A} = \Lambda \iint_{\Delta A'} \rho_d(x',y',t')\,dx'dy' \qquad (19)$$

The probability $P_{\Delta A}$, can be computed with Eq. (19), where the normalizing factor Λ is set so $P_{\Delta A} \rightarrow 1$ when $\Delta A' \rightarrow A'_{Total}$ (model total area) [4].

3.4 Model Parameters

All Dirac equation solutions herein use the following CGS parameters in the pde's: c = 2.998e10 cm/s, $\hbar = h/(2\pi)$ = 1.055e-27 cm^2-g/s and the particle (electron) mass m = 9.109e-28 g . Since these parameters are held fixed from problem to problem, the unprimed drive frequency ω is then governed by the remaining particle speed parameter β in Eq.(9).

4. Theory

The basic building blocks of the Dirac theory are freely propagating matter waves such as planar and cylindrical ones. For validation cross comparison purposes, exact solutions to these wave propagation problems are employed as either *time dependent transient* solutions (most difficult case therefore only available for plane wave case), or as *time independent steady state* limit reference solutions (where FEM vs exact comparisons are made <u>after enough time has past</u> so relative comparisons can be made).

4.1 Bar Transient Plane Wave (no gradual buildup of surface driver)

Initial FEM transient solutions showed some unusual buildup of the transition of the transient into the steady state solution. An exact closed form solution is needed to insure that this behavior is not due to some sort of computational anomaly. A two dimensional bar of length $L'=16$ is used as the computational domain (see Fig.(2a) inset). An exact solution $\Psi_1(x',t')$ is sought that meets pde Eq. (3), subject to *non-homogenous* BC: $\Psi_1(0,t')= \Psi_{10} \exp(-i\omega' t')$ & $\Psi_1(L',t')= 0$ for $t' \geq 0$ and IC's: Eqs. (17) for $0 \leq x' \leq L'$. The general method outlined in [5] for solving this type pde, converts the problem of solving a *homogenous pde* (zero rhs) with *non-homogenous* time driven BC's -into- having to solve a *non-homogenous pde* (nonzero rhs), with zero *homogenous* BC's. The newly converted pde is then solved with an *Eigenfunction expansion method*. The resulting solution is given by: (apply L'Hospital's limit rule to B_n if $a_n=\omega'$)

$$\Psi_1(x',t') = \Psi_{10}e^{-i\omega' t'}(1-x'/L') + \Psi_{10}(2/\pi)\sum_{n=1}^{n=\infty}\mathcal{T}_n(t')\sin(n\pi x'/L')$$

$$\mathcal{T}_n(t') = \frac{(\omega'^2-(c'M')^2)}{na_n}B_n - \frac{1}{n}\cos(a_n t') + \frac{i\omega'}{na_n}\sin(a_n t')$$

$$B_n = \frac{a_n e^{-i\omega' t'} - a_n\cos(a_n t') + i\omega'\sin(a_n t')}{a_n^2-\omega'^2};\ a_n = c'\sqrt{(n\pi/L')^2+M'^2}$$

Substituting Ψ_1 above into Eq.(5) easily gives Ψ_4. This same problem (with **3.4** model parameters, β =.67 and Ψ_{10} =1) was solved with the FEM, where a FEM-Exact comparison is shown in Fig.(2) as a sequence of time frames that illustrates the build up of the S.S. solution from the transient one (our time range of interest is <u>before</u> the wave hits the downfield B.C.). Note if $M'=0$ in Eq.(3), the wave equation would remain. Therefore d'Alembert's solution would be valid which implies the end driver wave form would travel undistorted down the bar. In contrast, for our $M'\neq 0$ case we track

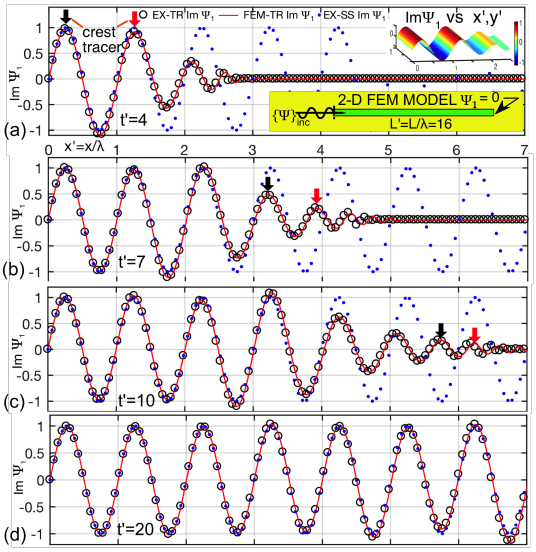

Figure 2. FEM vs Exact Wave Prop. vs x′ at 4 times

the development of the propagated driver wave form by observing the two black-red ⬇⬇ crest tracer arrows of Fig.(2a). Due to the dispersive M' term, both the amplitude reduces and peak-to-peak wave length changes in later frames Fig.(2b) and Fig.(2c). By frame Fig.(2d) at $t'=20$, the S.S. solution starts to take form (the S.S. limit is shown dotted in all 4 frames). The leading cycles (follow the crest tracers) melt away <u>*both in the FEM & Exact solutions*</u> as the wave propagates down the bar, thus showing this feature is not a numerical anomaly.

4.2 Effect of Gradual Surface Driver Buildup and Particle Velocity β on PW Propagation

The same FEM problem (except Eq.(16) B.C. is used downfield) treated in **4.1** is resolved, where the effect of surface driver gradual build up and particle velocity variations are considered here.

Gradual Driver Buildup: The upfield end face driver is the one used in Fig.(1a). The resulting FEM solution with gradual buildup (i.e. N_c=2) as compared to using no gradual buildup (i.e. N_c=0) is shown in Fig.(3b). Note the gradual buildup reduces the unwanted leading higher spatial frequency

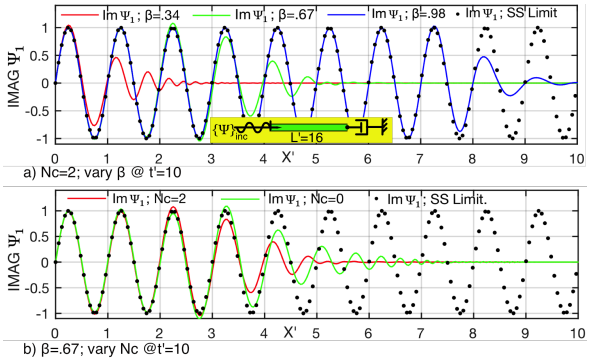

Figure 3. Variations of β and N_c on PW Solution

oscillations due to the suddenly applied Ψ_1 driver.

Variations on Particle Velocity: Fig.(3a) illustrates that the smaller the particle velocity (β parameter sweep={0.34, 0.67, 0.98}), the longer it takes for the steady state to build up. In later FEM demos, β=.98 is used to speed up reaching the S.S. limit.

4.3 Transient PW Reflection Validation

A FEM bar model (see Fig.(4a) inset), using **3.4** model parameters, β =.98, length L′ =8; with end driver represented by Eqs.(13-15), is solved. A snapshot in time (at t′=20) is shown in Fig.(4) after the transient wave has traveled down the bar and reflected off the back end hard $\partial\Psi_1/\partial x'$=0 B.C. . The exact transient solution is not available here, however the exact limiting steady state solution [2] is given by Eq.(20) and is shown as a background

$$\begin{Bmatrix}\Psi_1^T\\ \Psi_4^T\end{Bmatrix}_{EX} = A\underbrace{\begin{Bmatrix}1\\ 1\\ \overline{R'}\end{Bmatrix}e^{ik'x'-i\omega't'}}_{INCIDENT} + A\underbrace{\begin{Bmatrix}1\\ \frac{-1}{R'}\end{Bmatrix}e^{-ik'(x'-2L')-i\omega't'}}_{REFLECTED} \quad (20)$$

dotted curve in Fig.(4). The parameters in Eq.(20) are $\omega'=2\pi$, $k'=2\pi$, A=1, $R'=k'/[(\omega'/c')-M']$ =1.2067. After the incident wave interacts with the reflecting wave, there is a doubling of the incident wave peaks. This solution is important because it involves the interaction of two waves (incident with reflected) and also illustrates the accuracy of post processing Ψ_4 with Eq.(5) (e.g. Fig.(4b) .

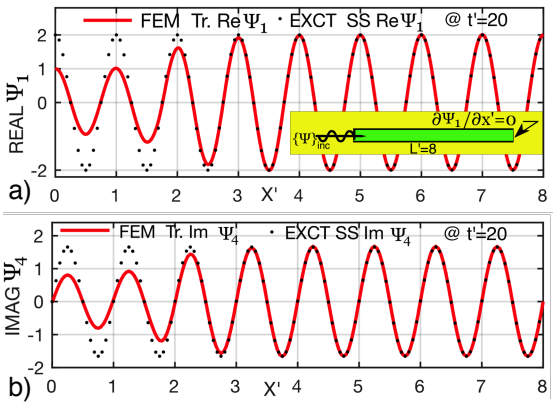

Figure 4. Transient PW Reflection From Hard BC

4.4 Transient Cylindrical Wave Validation

A 2-D cylindrical FEM annular region (of inner radius $R'_i = R_i/\mathbf{L}$ =4 and outer radius $R'_o = R_o/\mathbf{L}$ =9) is uniformly driven on the inside with Eqs.(13-15), using **3.4** model parameters, and particle velocity parameter β =0.98 . The outside surface is terminated with absorbing BC Eq.(16), where in [2] it was shown that at a large $k'\rho'$ argument=9, the outward traveling cylindrical wave absorbing BC is nearly the same as the PW boundary condition. As long as the dominant spatial frequency of the outward traveling wave is mostly monochromatic (e.g. like Fig.(1b)), Eq.(16) should work well even for a transient problem. In the absence of the exact transient solution, the next best thing is a comparison to the S.S. limit solution by running the FEM model out to say t′=9. The Eq. (21) exact S.S. limit solution for large $k'\rho'$ is given in [2,3] with A_0=1.0 , $R'=k'/[(\omega'/c')-M']$:

$$\begin{Bmatrix}\Psi_1(\rho',\varphi,t)\\ \Psi_4(\rho',\varphi,t)\end{Bmatrix} \approx A_0\begin{Bmatrix}1\\ \frac{exp[i\varphi]}{R'}\end{Bmatrix}\frac{exp[ik'\rho'-i\omega't']}{\sqrt{k'\rho'}} \quad (21)$$

where the angular coordinate φ and radial coordinate ρ ($\rho'=\rho/\mathbf{L}$), is shown in Fig.(5c) . The FEM solution compared to the S.S. solution limit (at time snapshot t′=9), is shown in Fig.(5) for the real part Ψ_1 and real part Ψ_4 of the wave function. The Fig.(5c-5d) comparison is significant, because even with a uniform Ψ_1 loading on the inner surface, the FEM solution using the post processing Eq.(5), picked up the Ψ_4 spiral variation in φ with good agreement between the FEM and Exact S.S. limit solution. Finally Fig.(6) displays good FEM↔Exact *S.S.* radial line plot comparisons of re Ψ_1 , im Ψ_1 , re Ψ_4 , im Ψ_4 at fixed angles **of** φ=-45˚ and -135˚.

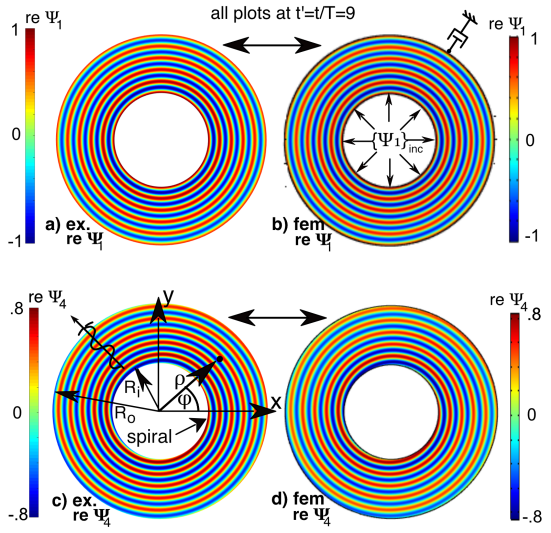

Figure 5. Transient Cylindrical Wave 2-D Carpet Plot

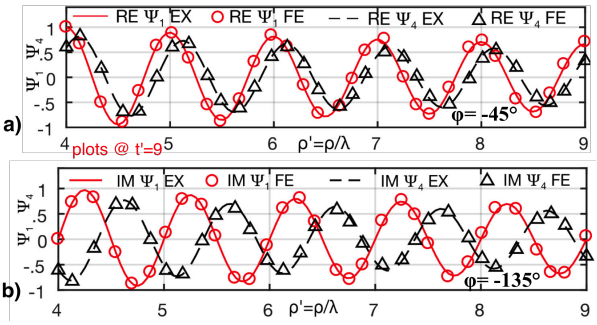

Figure 6. Transient Cylindrical Wave Radial Variation

5. Results for More Complex FEM Models

More complex FEM models are presented here where there is no exact reference solution (either transient or S.S. limit) available.

5.1 Multiple Cylinder Reflections

The purpose of this exercise is to illustrate the reflection of Dirac waves off of multiple surfaces. Firstly, a plane wave is incident upon a single cylinder (with hard BC condition iii) of diameter d′=2, where the wave is initiated by driving the left upfield face with Eqs.(13-15), using **3.4** model parameters, and particle velocity parameter β =0.98 . The resulting $|\Psi_1|$ FEM solution at fixed time (t′=20) is shown in Fig.(7a). Next, the same setup is used except the incident wave impinges upon three cylinders, all of diameter d′=2, with spacing $D'_x=\sqrt{12}$, $D'_y=8$, where the resulting interactions are shown in Fig.(7b). The Fig.(7c) case is exactly the same as the Fig. (7b) one except the vertical spacing is smaller by a factor of two ,

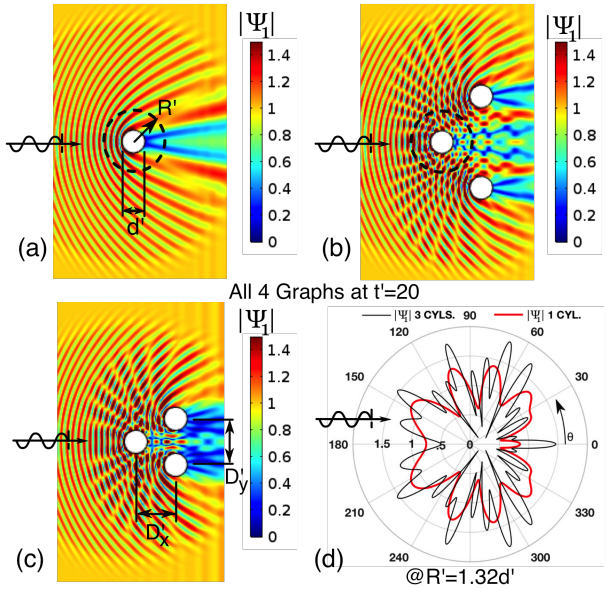

Figure 7. Transient PW incident cylinder cluster

namely $D'_x=\sqrt{12}$, $D'_y=4$. In Fig.(7d), a polar plot comparison is made at radius R′=√7 (i.e. at dashed circle in Fig.(7a) and (7b)), that compares the $|\Psi_1|$ results of Fig.(7a) and Fig.(7b). Due to the constructive and destructive interactions of wave reflections off the back cylindrical surfaces, there is much more activity in the peaks and nulls of the 3 cylinder case compared to the 1 cylinder case.

5.2 Transient Double Slit Demonstration

A classic demonstration of quantum mechanics is the two slit experiment. The downfield location of an incident particle fired at the slits is simulated by passing a transient PW through two slits. The wave is initiated by driving the slit portals with Eqs.(13-15), (using **3.4** model parameters, and particle velocity parameter β =0.98). Using the notation in the Fig.(8a) slit inset detail, the model parameters are: aperture a′=a/**L**=0.5, slits center to center pitch p′=p/**L**=4, and entrance slit tunnel length d′=d/**L**=0.2 . Two snapshots in time (at t′=4.1 and t′=12.2) are shown in Fig.(8a) and Fig.(8b) respectively, where the downfield spreading of the two (real pt Ψ_1) waves emanating from the slits is clearly displayed. The Fig.(8c) plot of $|\Psi_1|$, at t′=20 , illustrates the formation of alternating bands of constructive and destructive interference. A closer look at the interference pattern is obtained by taking a vertical slice at x′=1.9 (labeled in Fig. (8c)), when t′=20, and plotting the Eq.(18) probability density ρ_d vs y′ (the results for Ψ_4 were

obtained with Eq.(5)). Note, the ratio of the ρ_{IL} "*in line with slit*" probability density -to- the ρ_{OL} "*average off line*" probability density is ρ_{IL}/ρ_{OL} =

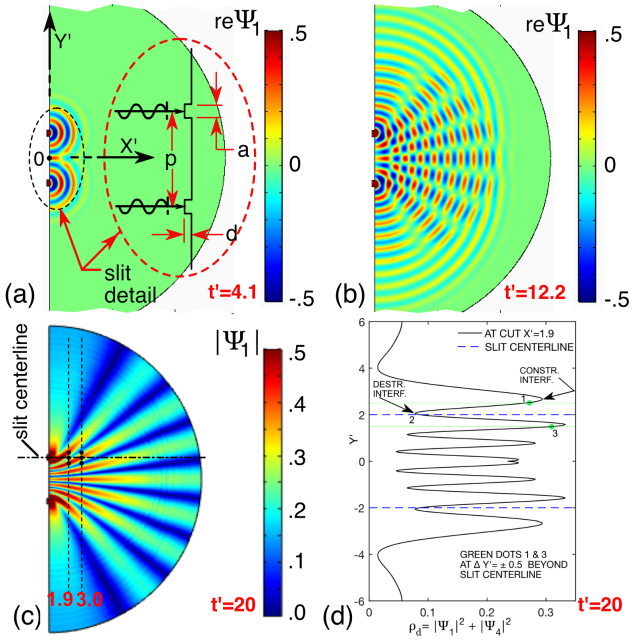

Figure 8. Transient Double Slit Demonstration

0.272 (see measurement points 1,2,3 in Fig.(8d) where $\rho_{IL}\equiv\rho_{d2}$ and $\rho_{OL}\equiv(\rho_{d1}+\rho_{d3})/2$ is the avg. at $\Delta y'=\pm.5$). Thus the probability density for a particle being in line with the slit is 0.272 times smaller than being off line. This is significant because it shows at the atomic scale, particles can behave like waves having destructive interference. One might otherwise intuitively expect that it is more likely to have the particle location (after going through the slit) be inline with the slit like one would have with large non atomic scale masses passing through a large slit. The bands are not parallel to the slits, thus at another cut ($x'=3$ of Fig.(8c)), ρ_{IL}/ρ_{OL} =11.8, hence here the constructive interference probability density for a particle being in line with the slit is 11.8 times greater than being $\Delta y'=\pm.5$ off line.

5.3 Steady State Double Slit Demonstration

Here a two slit problem is solved as a *time independent* problem, where unlike [2] that used the S.S. version of coupled Eqs.(2), the uncoupled S.S. equations Eqs.(7-8) are used here instead. For comparative purposes, the same model used in [2] (except for bigger outer boundary truncation radius) is resolved here. The wave is initiated by driving slit portals with $\psi_1(t')= 1.0\exp(-i\omega' t')$, using **3.4** model parameters, and particle velocity parameter β =0.34 . The slit model parameters are: aperture $a'=1/12$, slit pitch $p'=2$, and $d'=0$. The radial outer boundary is terminated at $R'=14$ with cylindrical wave absorbers described in [2]. A same scale $|\psi_1|$ comparison between the reference [2] Fig.(9b) solution (using the coupled first order formulation) and the Fig.(9a) solution (using Eqs. (7-8) uncoupled formulation) is given in Fig.(9). The uncoupled solution appears to be smoother. This could be partly due to the larger R' outer boundary placement ($R'=14$ vs $R'=5$).

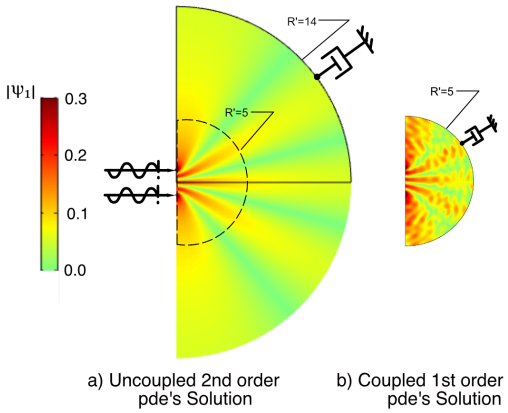

9. Steady State Double Slit Demonstration

6. Conclusions

There is good agreement between exact vs FEM solutions for three validation examples. The transient formulation has the advantageous option of solution termination before having to deal with absorbing boundaries. Solution to the incident harmonic wave function upon a two slit barrier, produced diffraction patterns showing null zone bands due to wave destructive interference, thus showing the wave like behavior of particles at the atomic scale. Post processing the Ψ_4 component from the solved (i.e. stored) $\partial\Psi_1/\partial x'$, $\partial\Psi_1/\partial y'$ spatial derivatives did not lead to any numerical difficulties for either the transient or steady state formulations .

7. References

[1] Paul Strange, Relativistic Quantum Mechanics, Camb. Univ. Press Cambridge 1998.

[2] A.J. Kalinowski,"Relativistic Quantum Mechanics Applicat. Using The Time Independent Dirac Equation" ,COMSOL Conf. Proc, 2016.

[3] G.F. Torres, et al., "Solution of Nonscaler Eqs." ,Revista Mex. de Fisica **38**, No 1 (1992).

[4] A.J. Kalinowski,"Quantum Mechanics Applications Using the Time Dependent Schrödinger Eq.", COMSOL Conf. Proc, 2015.

[5] Philippe Laval, *PDE's for Scientist Notes 2009*.